Probing dielectric-response effects with attosecond time-resolved streaked photoelectron spectroscopy of metal surfaces

C.-H. Zhang and U. Thumm
Department of Physics, Kansas State University, Manhattan, Kansas 66506, USA
(Received 3 February 2011; published 2 December 2011)

The release of conduction-band electrons from a metal surface by a subfemtosecond extreme ultraviolet (XUV) pulse and their propagation through the solid provoke a dielectric response in the solid that acts back on the photoelectron wave packet. We calculated the (wake) potential associated with this photoelectron self-interaction in terms of bulk and surface plasmon excitations and show that it induces a considerable, XUV-frequency-dependent temporal shift in laser-streaked XUV photoemission spectra, suggesting the observation of the ultrafast solid-state dielectric response in contemporary streaked photoemission experiments.

DOI: 10.1103/PhysRevA.84.063403 PACS number(s): 33.80.Wz, 78.66.Bz, 42.65.Re, 78.47.J−

I. INTRODUCTION

Owing to significant progress in laser technology over the past decade, subfemtosecond extreme ultraviolet (XUV) pulses can now be generated and synchronized with a primary infrared (IR) laser pulse, allowing the time-resolved observation of the electronic dynamics in atoms [1] and solids [2]. Time-resolved experiments at the intrinsic time scales of an active electron and the correlated dynamics of two electrons [3,4] or plasmons [5,6] promise unprecedented sensitive experimental tests of collective electronic phenomena in solids and novel plasmonic devices [7,8] and are relevant for promoting applications to energy conversion and medicine within the emerging field of nanoplasmonics [9].

Using attosecond time-resolved XUV + IR pump-probe technology in a proof-of-principle experiment, a relative temporal shift of 110 as (1 as $= 10^{-18}$ s) between photoemission of the $4f$ core level and conduction-band electrons from a tungsten (110) surface was recently measured [2]. Essential for the correct reproduction of this shift within quantum mechanical models [10,11] is the proper inclusion of (i) the photoelectron's (PE's) phase evolution in the IR laser field during streaked emission, (ii) the attenuation of the IR pulse inside the solid (skin effect), and (iii) PE transport effects in the solid [12,13]. The release and subsequent motion of the PE in and in front of a solid dielectric medium provoke collective electron excitations in the solid. These induced wave-like electron-density fluctuations appear since the electron distribution in the solid cannot equilibrate during the motion of the released PE. They depend on the kinetic energy E of the PE.

For a given dielectric response function $\epsilon(\vec{Q},\omega)$ these induced charge-density fluctuations can be related to a scalar complex-valued effective potential, the so-called "wake potential," by solving Poisson's equation within the specular-reflection model [14,15]. The real part of the wake potential is due to virtual bulk and surface excitations, while its imaginary part accounts for inelastic scattering and energy loss or gain of the PE. Evaluated at the position of the PE, the wake potential leads (up to a factor of $1/2$) to the self-energy of the PE [14,16–18]. The self-energy thus amounts to a complex-valued dynamic image potential that represents the back-interaction of induced collective bulk and surface excitations of the substrate on the PE itself. This plasmon-mediated self-image interaction affects the motion of the PE, in particular, its phase. It therefore alters relative temporal shifts in photoemission and absolute photoemission time delays [1,19].

The dependence of the dynamic wake potential on the charge state and velocity of the wake-inducing particle has been studied with regard to energy loss [20,21], electron-exchange and -correlation contributions [22], electron emission in ion-surface collisions [23], and electronic self-interaction effects on PE spectra [15]. While these examples emphasize the influence of the solid's dielectric response, they do not resolve the ultrafast electronic response in the condensed-matter-plus-charged-particle system in time. In this work we extend previous theoretical studies on the streaked photoemission from surfaces [10,13,24,25] to expose the effect of the dynamic plasmon response on time-resolved PE spectra, suggesting the study of many-body processes in solids in streaked PE emission experiments [2].

This paper is organized as follows. In Sec. II, we present the underlying theoretical model to calculate the dynamic self-image potential of a PE. In this section, we use second-quantization techniques to account for the creation and destruction of surface and bulk plasmon modes, closely following previous theoretical work [15,18,20,22,26]. In Sec. III, we employ the effective dynamic image potential derived in the previous section and solve the single-electron time-dependent Schrödinger equation (TDSE) to obtain IR-streaked XUV PE spectra from a jellium metal surface. In Sec. IV, we compare our TDSE results with and without the inclusion of dynamical plasmon-response effects. Our conclusions follow in Sec. V. Unless indicated otherwise, we use atomic units (a.u.) throughout this work.

II. DYNAMIC IMAGE POTENTIAL

The dielectric response of conduction electrons to a released PE is a complex quantum-mechanical many-body problem [15]: The dynamic image potential effect on the motion of PEs is a self-interaction process. The release and motion of a PE induce a collective response of the substrate's conduction electrons that involves the dynamical creation and annihilation of surface and bulk plasmon modes and electron-hole pairs. These substrate excitations, in turn, act back on the PE, leading to an effective "self-interaction" of the released PE that can

be accounted for by the self-energy $\Sigma(\mathbf{r})$. The net effective potential of a PE at position $\mathbf{r}$ is thus given by an effective single-particle potential,

$$U(\mathbf{r}) = U_0(\mathbf{r}) + \Sigma(\mathbf{r}), \tag{1}$$

where $U_0(\mathbf{r})$ is the undisturbed single-particle potential for the electrons of the solid target. The complex-valued self-energy $\Sigma = \Sigma_r + i\,\Sigma_i$ depends on the characteristics of the released PE and the electronic properties of the substrate. Its real part Σ_r models the virtual excitation of electron-hole pairs and collective electron excitations (plasmons), while its imaginary part Σ_i accounts for a net energy transfer between the PE and collective modes of the substrate. Therefore, Σ_i presents the inelastic scattering of the PE during its propagation to the detector.

In view of the convoluted nature of this self-interaction process, the actual calculation of Σ requests approximations. In order to calculate the dynamic effective plasmon-response potential for photoemission from a metal surface, we orient the z axis of our coordinate system along the surface normal and toward the vacuum side and assume that the released PE moves with a constant velocity $v_z > 0$ along a classical trajectory toward the surface and crosses the metal-vacuum interface at $z = 0$ at time $t = 0$. The classical motion of the PE is thus given by the charge density $\rho(\mathbf{r}) = \delta(\mathbf{r}_\parallel)\delta(z - v_z t)$.

Depending on its kinetic energy, there are four possible processes that contribute to the PE inelastic scattering: electron-phonon interactions at low energy, electron-electron interactions (dielectric response), interband transitions, and secondary core-level photoionization or Auger processes at high energy [12,13]. In typical streaking experiments, the kinetic energy of PEs is of the order of 10–100 eV, and inelastic scattering is mainly due to electron-electron interactions. An elementary approach to including inelastic interactions between the PE and the substrate is to add an imaginary part $\kappa = 1/2\lambda$ to the PE momentum, where λ is the PE mean-free path [10,27]. This is equivalent to assuming a purely imaginary self-energy,

$$\Sigma(z, v_z) \approx i\,\Sigma_{\rm ph}(z, v_z) = -i\,v_z/(2\lambda)\Theta(-z), \tag{2}$$

where $\Theta(z)$ is the unit step function. The nonzero value of λ implies that only PEs that originate within a distant from the surface of a few times λ contribute to the photocurrent.

We model the semi-infinite-solid-in-jellium approximation with the potential

$$U_0(\mathbf{r}) = U_J(z) = -\frac{V_0}{1 + e^{z/a}}, \tag{3}$$

where V_0 is the height of the potential step at the metal-vacuum interface and a defines the thickness of the interface region. We use the following dielectric function to describe bulk plasmon and particle-hole excitations [18]:

$$\epsilon_B(\mathbf{k},\omega) = 1 + \frac{\omega_p^2}{3k_F^2k^2/5 + k^4/4 - \omega(\omega + i\gamma)}. \tag{4}$$

It entails the dispersion relation

$$\omega_{\mathbf{k}}^2 = \omega_p^2 + 3k_F^2k^2/5 + k^4/4. \tag{5}$$

An approximate expression for the surface dielectric function could be derived from the bulk dielectric properties [28]. Instead, we adopt the surface-plasmon-pole approximation of Echenique *et al.* [26] and model surface-plasmon and particle-hole excitations with the surface dielectric function [18]

$$\epsilon_S(\mathbf{Q},\omega) = 1 + \frac{\omega_p^2}{\omega^2 - \omega_p^2 - \alpha Q - \beta Q^2 - Q^4/4}, \tag{6}$$

which gives the surface plasmon dispersion relation

$$\omega_{\mathbf{Q}}^2 = \omega_p^2/2 + \alpha Q + \beta Q^2 + Q^4/4. \tag{7}$$

For low momenta $\mathbf{k} = (\mathbf{Q}, k_z)$, these dispersion relations model single-plasmon modes with bulk- and surface-plasmon frequencies $\omega_p^2 = 4\pi n$ and $\omega_s = \omega_p/\sqrt{2}$, respectively. Here n is the bulk conduction-electron density and $k_F = (3\pi^2 n)^{1/3}$ the Fermi velocity. The decay of these modes into particle-hole pair excitations at high momenta is modeled through the k^4 and Q^4 terms. The parameter $\alpha = \sqrt{3}k_F\omega_p/\sqrt{10}$, and β is determined so that the surface- and bulk-plasmon dispersion curves join the particle-hole continuum at the same point (same momentum and energy) [26]. With these approximations, the plasmon field of the undistorted solid is represented by the free Hamiltonian

$$H_0 = \sum_{\mathbf{Q},k_z\geqslant 0} \omega_k b_{\mathbf{k}}^\dagger b_{\mathbf{k}} + \sum_{\mathbf{Q}} \omega_Q a_{\mathbf{Q}}^\dagger a_{\mathbf{Q}}, \tag{8}$$

where $b_{\mathbf{Q}}^{(\dagger)}$ and $a_{\mathbf{k}}^{(\dagger)}$ are annihilation (creation) operators for bulk and surface plasmons, respectively [15,20,22].

The interaction between the (classical) PE and the solid is given by the interaction Hamiltonian

$$H_1 = \int d\mathbf{r}\rho(\mathbf{r})[\phi_b(\mathbf{r}) + \phi_s(\mathbf{r})] \tag{9}$$

in terms of the bulk- and surface-plasmon fields [15]

$$\phi_b(\mathbf{r}) = \sum_{\mathbf{Q},k_z\geqslant 0} B_{\mathbf{k}} b_{\mathbf{k}} \sin(k_z z) e^{i\mathbf{Q}\cdot\mathbf{r}_\parallel}\Theta(-z) + \text{H.c.}, \tag{10}$$

$$\phi_s(\mathbf{r}) = \sum_{\mathbf{Q}} A_{\mathbf{Q}} a_{\mathbf{Q}} e^{-Q|z|} e^{i\mathbf{Q}\cdot\mathbf{r}_\parallel} + \text{H.c.}, \tag{11}$$

with interaction strengths

$$|B_{\mathbf{k}}|^2 = 8\pi\omega_p^2/(Vk^2\omega_k), \tag{12}$$

$$|A_{\mathbf{Q}}|^2 = \pi\omega_s^2/(SQ\omega_Q), \tag{13}$$

quantization volume V, and quantization surface S, respectively. The bulk-plasmon field in Eq. (10) vanishes at the surface and in the vacuum, and the surface-plasmon field is chosen so that its value inside the solid is a reflection of its value in the vacuum (specular-reflection model).

The total Hamiltonian

$$H = H_0 + H_1 \tag{14}$$

describes the interaction of the bulk- and surface-plasmon fields of the substrate with a uniformly moving classical PE.

A given initial state of the plasmon field, $|\psi(-\infty)\rangle$, evolves according to

$$|\psi(t)\rangle = \mathrm{T}\exp\left[-i\int_{-\infty}^{t} H_{1,I}(t')dt'\right]|\psi(-\infty)\rangle, \quad (15)$$

where T is the time-ordering operator and

$$H_{1,I}(t) = e^{iH_0 t} H_1 e^{-iH_0 t} \quad (16)$$

is the interaction-picture representation of H_1. In our application, $|\psi(-\infty)\rangle$ is given as the vacuum state of the plasmon field, and its time evolution can be carried out exactly [20,21].

The complex self-energy of the interacting PE can now be calculated as

$$\Sigma(t,v_z) = \tfrac{1}{2}\langle\psi(t)|H_{1,I}(t)|\psi(t)\rangle = \Sigma_b(t,v_z)+\Sigma_s(t,v_z), \quad (17)$$

with a bulk contribution $\Sigma_b(t,v_z)$ and a surface contribution $\Sigma_s(t,v_z)$. Following Refs. [18], [22], and [26] for the special case of photoemission perpendicular to the surface and using the conversion $t = z/v_z$, we obtain the bulk contribution to the self-energy

$$\Sigma_b(z,v_z) = -\frac{2\Theta(-z)}{\pi}\int_0^\infty \frac{dk}{k}\int_0^k dk_z\left[\frac{1}{\epsilon_B(k,\omega=k_z v_z)}-1\right] \times \sin^2(k_z z) = \Sigma_{b,r} + i\Sigma_{b,i}, \quad (18)$$

with the real and imaginary parts

$$\Sigma_{b,r}(z,v_z) = \frac{\Theta(-z)\omega_p^2}{\pi}\int_0^\infty\frac{dk}{k} \times \int_0^k dk_z \frac{(k_z^2v_z^2-\omega_k^2)[1-\cos(2k_z z)]}{(k_z^2v_z^2-\omega_k^2)^2+k_z^2v_z^2\gamma^2}, \quad (19)$$

$$\Sigma_{b,i}(z,v_z) = -\frac{\Theta(-z)v_z\omega_p^2\gamma}{\pi}\int_0^\infty\frac{dk}{k} \times \int_0^k dk_z \frac{2k_z[1-\cos(2k_z z)]}{(k_z^2v_z^2-\omega_k^2)^2+k_z^2v_z^2\gamma^2}. \quad (20)$$

Similarly, the real part of the surface contribution to the self-energy follows as

$$\begin{aligned}\Sigma_{s,r}(z,v_z) &= \frac{1}{2}\int_0^\infty dQ\ \Xi_s(Q,v_z)e^{-2Q|z|} \\ &\quad +\Theta(z)v_z\int_0^\infty\frac{dQ\,Q}{\omega_Q}\Xi_s(Q,v_z)e^{-Qz}\sin(\omega_Q z/v_z) \\ &= -\frac{\omega_s^2}{2}\int_0^\infty\frac{dQ}{Q^2v_z^2+\omega_Q^2}e^{-2Q|z|} - \Theta(z)v_z\omega_s^2 \\ &\quad \times\int_0^\infty\frac{dQ}{\omega_Q(Q^2v_z^2+\omega_Q^2)}e^{-Qz}\sin(\omega_Q z/v_z),\end{aligned} \quad (21)$$

with the definition

$$\Xi_s(Q,v_z) = \frac{\epsilon_S(Q,\omega=iQv_z)-1}{\epsilon_S(Q,\omega=iQv_z)+1}. \quad (22)$$

However, the specular-reflection method used above does not provide the imaginary part $\Sigma_{s,i}(z,v_z)$. Physically, $\Sigma_{s,i}(z,v_z)$ represents the rate of creating surface plasmons. Accordingly, it can be obtained from the energy lost by the PE to surface excitations, resulting in [26]

$$\Sigma_{s,i}(z,v_z) = -\frac{v_z\omega_s^2}{2}\int_0^\infty\frac{dQ\,Q}{\omega_Q(\omega_Q^2+Q^2v_z^2)}[\Theta(-z)e^{-2Q|z|} + \Theta(z)\{2\cos(\omega_Q z/v_z)e^{-Qz}-e^{-2Qz}\}]. \quad (23)$$

The real part of $\Sigma(z,v_z)$ converges to the classical self-image potential $\Sigma_r(z,v_z)\to -1/4z$ as $z\to\infty$ for all values of v_z [29,30]. For $v_z\to 0$, $\Sigma(z,v_z)$ approaches the static limit

$$\Sigma(z,v_z=0) = \Sigma_r(z) = -\frac{2\Theta(-z)\omega_p^2}{\pi}\int_0^\infty\frac{dk}{k}\int_0^k dk_z\frac{\sin^2(k_z z)}{\omega_k^2} - \frac{\omega_s^2}{2}\int_0^\infty dQ\frac{e^{-2Q|z|}}{\omega_Q^2}. \quad (24)$$

We point out that $\Sigma_i(z,v_z)$ is approximately proportional to v_z, consistent with the phenomenological expression in Eq. (2). The comparison of Eq. (2) with $\Sigma_i(z,v_z)=\Sigma_{b,i}(z,v_z)+\Sigma_{s,i}(z,v_z)$ can thus be used to define an effective, z-dependent mean-free path $\lambda(z)$. Since $\Sigma_i(z,v_z)$ vanishes at $v_z=0$, $\Sigma(z,v_z=0)$ is real, such that $U_J(z)+\Sigma(z,v_z=0)$ is, in jellium approximation, the effective binding potential for an electron in the metal. Therefore, we need to adjust the parameters in U_J so that $U_J(z)+\Sigma(z,v_z=0)$ gives the correct Fermi energy.

Figure 1(a) shows $\Sigma_r(z,v_z)$ for different PE velocities v_z for aluminum with $\omega_s = 0.378$, $\omega_p=\sqrt{2}\omega_s$, and $\gamma=0.1\omega_p$. We adjust the potential step to $V_0 = 10.2$ eV and the interface-thickness parameter to $a = 1.4$ Å, respectively, in order to reproduce the Fermi energy of aluminum, $\varepsilon_F = 11.7$ eV [Fig. 1(b)]. For $v_z>0$, $\Sigma_r(z,v_z)$ oscillates near the metal surface with wavelength $\lambda_b = \pi v_z/\omega_p$ inside the solid and $\lambda_s = 2\pi v_z/\omega_s$ in the vacuum. Our numerical results confirm that it approaches $-1/4z$ [30] far away from the surface for all v_z, as expected and mentioned above. In the static limit, indicated as "$v_z=0$," $\Sigma_r(z,v_z=0)$ becomes constant inside

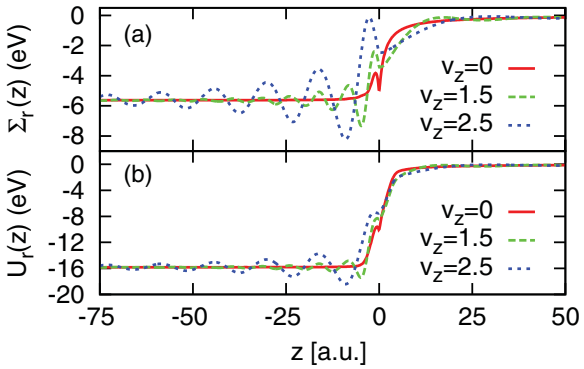

FIG. 1. (Color online) (a) Dynamic wake potential $\Sigma_r(z,v_z)$ for aluminum for different PE velocities v_z. (b) Real part of the potential $U(z,v_z)=U_J(z)+\Sigma(z,v_z)$. The parameters a and V_0 in the jellium potential U_J [cf. Eq. (2)] are adjusted such that $U(z\to-\infty,v_z=0)$ equals the bulk limit ϵ_F+W, where ϵ_F and W are the Fermi energy and work function, respectively, for aluminum. The curves shown in (a) and (b) for $v_z\neq 0$ are normalized to the respective $v_z=0$ bulk limits.

the solid and approaches $-1/4z$ for large z on the vacuum side. The "kink" near $z = 0$ in the self-energy $\Sigma(z, v_z)$ arises since only the continuity of the plasmon field, and not the continuity of its derivative, is imposed at $z = 0$ within the specular-reflection model [15].

III. TIME-DEPENDENT SCHRÖDINGER EQUATION

We model the metal surface as a 300-a.u.-wide slab and obtain its eigenvectors ε_n and wave functions $\Phi_n(z)$ by diagonalizing the TDSE

$$\varepsilon_n \Phi_n(z) = \left[-\frac{1}{2}\frac{d^2}{dz^2} + U_J(z) + \Sigma(z, v_z = 0)\right]\Phi_n(z). \quad (25)$$

By increasing the slab thickness to 450 a.u., we found that the numerical results in the following figures in this work show no discernible change with regard to calculations for the 300-a.u.-wide slab. We represent the vector potential of the laser pulse as

$$A_L(z,t) = A_0 \sin^2(\pi t/\tau_L)\cos[\omega_L(t - \tau_L/2)] \times [e^{z/\delta_L}\Theta(-z) + \Theta(z)] \quad (26)$$

for $0 \leqslant t \leqslant \tau_L$ and 0 otherwise, with $\hbar\omega_L = 1.57$ eV, peak intensity $I_L = A_0^2\omega_L^2/2 = 5 \times 10^{11}\mathrm{W/cm^2}$, and pulse length $\tau_L = 8$ fs. We include an exponential damping of the IR laser field inside the solid with skin depth δ_L and assume a Gaussian XUV pulse,

$$E_X(t) = E_{X,0}e^{-2\ln 2(t/\tau_X)^2}\cos(\omega_X t), \quad (27)$$

with pulse length $\tau_X = 300$ as. In typical streaking experiments, the XUV-pulse peak intensity $I_X = E_{X,0}^2$ is sufficiently low that photoemission in the XUV pulse can be treated perturbatively.

In order to investigate the influence of the dynamical plasmon response on photoemission spectra and time delays, we distinguish the following three cases.

A. Static image potential with phenomelogical modeling of Σ_i

We describe the release and propagation of the PE wave packet $\delta\psi_n(z,t)$ from occupied substrate states $\psi_n(z,t)$ by solving the TDSE [11],

$$i\frac{\partial}{\partial t}\delta\psi_n(z,t;\tau) = H_{L,\mathrm{sta}}(t)\delta\psi_n(z,t;\tau) + zE_X(t+\tau)\psi_n(z,t), \quad (28)$$

where

$$H_{L,\mathrm{sta}} = \frac{1}{2}\left[-i\frac{d}{dz} + A_L(z,t)\right]^2 + U_J(z) + \Sigma_r(z, v_z = 0) + i\Sigma_{\mathrm{ph}}(z, v_z) \quad (29)$$

is the Hamiltonian for the solid slab including the static image potential in $U_J(z) + \Sigma_r(z, v_z = 0)$ in the presence of the IR-laser pulse $A_L(z,t)$. $v_z = \sqrt{2(\omega_X - |\varepsilon_n|)}$ is the speed of the PE. Using $\Sigma_{\mathrm{ph}}(z, v_z)$ from Eq. (2) we include the damping of the PE and denote the results of this calculation as "static."

The delay τ between the XUV and the IR pulses is assumed to be positive if the XUV pulse precedes the IR pulse. The evolution of the nth initial state below the Fermi surface in the IR pulse is given by

$$i\frac{\partial}{\partial t}\psi_n(z,t) = H_{L,\mathrm{sta}}(t)\psi_n(z,t). \quad (30)$$

Since $E_{L(X)}(t \to \pm\infty) = 0$, Eqs. (28) and (30) are solved for the initial conditions $\delta\psi_n(z, t \to -\infty; \tau) = 0$ and $\psi_n(z, t \to -\infty) = \Phi_n(z)e^{-i\varepsilon_n t}$. This "static" calculation does not include wake effects that are due to the dielectric response of the substrate *during* the motion of the PE in the *real* part of the self-energy $\Sigma(z, v_z \neq 0)$. Using results of the static calculation as a reference will allow us to expose effects due to the dynamic dielectric response of the substrate on streaked photoemission spectra (see Sec. IV).

B. Dynamic image potential with phenomelogical modeling of Σ_i

In order to include the dynamical plasmon response to the moving PE, we replace the Hamilitonian $H_{L,\mathrm{sta}}(t)$ in Eq. (29) by

$$H_{L,\mathrm{dyn-ph}} = \frac{1}{2}\left[-i\frac{d}{dz} + A_L(z,t)\right]^2 + U_J(z) + \Sigma_r(z, v_z) + i\Sigma_{\mathrm{ph}}(z, v_z). \quad (31)$$

We designate the results obtained with this Hamiltonian as "dynamic-phenomenological" (dyn-ph). As in the previous subsection, the damping effect of the PE is still described phenomenologically by $\Sigma_{\mathrm{ph}}(z, v_z)$, but now the effect of the plasmon dynamics generated by the moving PE ("wake effect") is included in the real part of the complex self-energy $\Sigma(z, v_z)$. The comparison of this dyn-ph result with the static result therefore reveals the influence of dynamical response effects in the substrate charge distribution on the PE. The evolution of the nth initial state below the Fermi surface in the IR pulse is still given by Eq. (30).

C. Full dynamic image potential

Including the full complex-valued dynamical image potential $\Sigma(z, v_z)$ in the Hamiltonian

$$H_{L,\mathrm{dyn}} = \frac{1}{2}\left[-i\frac{d}{dz} + A_L(z,t)\right]^2 + U_J(z) + \Sigma(z, v_z), \quad (32)$$

we obtain results that we refer to as "fully dynamic" (dyn).

For each of the three cases distinguished above, we obtain a corresponding PE wave packet $\delta\psi_n(z,t;\tau)$. Assuming free-electron dispersion, $E = k^2/2$, the energy-differential photoemission probability

$$P(E,\tau) = \sum_{\varepsilon_n < \varepsilon_F} |\delta\tilde{\psi}_n(k,\tau)|^2 \quad (33)$$

leads to the delay-dependent center of energy (COE) of the PE spectrum,

$$E_{\mathrm{COE}}(\tau) = \frac{1}{2P_{\mathrm{tot}}(\tau)}\sum_{\varepsilon_n < \varepsilon_F}\int dk |k\,\delta\tilde{\psi}_n(k,\tau)|^2, \quad (34)$$

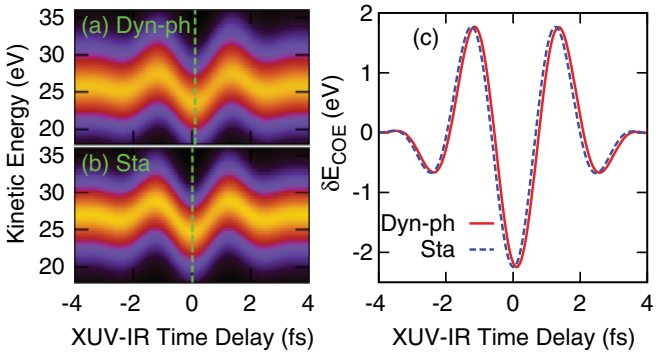

FIG. 2. (Color online) Streaked PE spectra for an aluminum surface calculated with (a) the dynamic image potential and (b) the static image potential for $\hbar\omega_X = 40$ eV, $\delta_L = 0$, and the PE mean-free path $\lambda = 5$ Å. (c) Corresponding centers of energy $E_{\rm COE}$. The relative temporal shift between the streaking traces for dynamic and static image potentials amounts to 100 as.

where $\delta\tilde{\psi}_n(k,\tau)$ is the Fourier transform of $\delta\psi_n(z,t\to\infty;\tau)$ and

$$P_{\rm tot}(\tau) = \sum_{\varepsilon_n<\varepsilon_F} \int dk |\delta\tilde{\psi}_n(k,\tau)|^2 \tag{35}$$

is the total emission probability. We define temporal shifts $\Delta\tau$ for static (dynamic) calculations relative to A_L by fitting [10,11]

$$E_{\rm COE}(\tau) = a + bA_L(\tau - \Delta\tau). \tag{36}$$

IV. RESULTS

We first present results for $\delta_L = 0$ for which the IR field is completely screened inside the solid. In Fig. 2 we compare the static and dynamic (dyn-ph) streaked PE spectra and their centers of energies for $\hbar\omega_X = 40$ eV. We determine the corresponding temporal shifts $\tau_{\rm sta(dyn-ph)}$ according to Eq. (36). Figure 2(c) shows the relative temporal shift $\Delta\tau_{\rm wake} = \Delta\tau_{\rm dyn-ph} - \Delta\tau_{\rm sta} \approx 100$ as, suggesting a noticeable—on the scale of the temporal resolution achievable in measured streaked PE spectra—contribution of the dynamical plasmon response to the photoemission delay.

Our results for $\Delta\tau_{\rm dyn-ph}$ and $\Delta\tau_{\rm sta}$ as a function of $\hbar\omega_X$ between 30 and 100 eV shown in Fig. 3(a) reveal that the dynamical plasmon response in the substrate has a significant effect on the PE delay, especially for $\hbar\omega_X < 50$ eV, where $\Delta\tau_{\rm dyn-ph}$ develops a double-hump structure. The ω_X dependence of $\Delta\tau_{\rm wake}$ can be understood as a result of the scattering of PEs in the self-interaction potential $\Sigma_r(z,v_z)$. This interaction of the PE changes the phase of $\delta\psi_n(z,t)$, giving rise to a "Wigner delay" $\Delta\tau^W$ [19,31].

Not including the effect of the streaking IR-laser field, we determine the Wigner delays $\Delta\tau^W_{\rm sta(dyn-ph)}$ from the PE position

$$\langle z\rangle = \int dkz |\delta\psi_n(z,t)|^2 \tag{37}$$

and velocity

$$\langle v\rangle = \int dk |k\delta\psi_n(k,t)|^2 \tag{38}$$

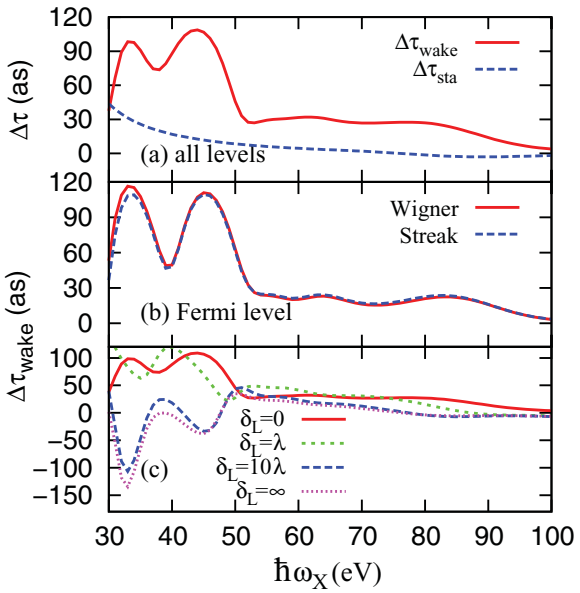

FIG. 3. (Color online) (a) $\Delta\tau_{\rm wake} = \Delta\tau_{\rm dyn-ph} - \Delta\tau_{\rm sta}$ and $\Delta\tau_{\rm sta}$ as functions of the XUV frequency obtained by fitting Eq. (36) to the calculated $E_{\rm COE}(\tau)$, including all levels below the Fermi surface and for the IR skin depth $\delta_L = 0$. (b) Comparison of $\Delta\tau_{\rm wake}$, obtained from $E_{\rm COE}(\tau)$ for the emission of PEs from the Fermi surface, with the Wigner delay $\Delta\tau^W_{\rm wake}$. (c) $\Delta\tau_{\rm wake}$ at different IR penetration depths.

at a time $t \gg \tau_L$ according to

$$\langle z\rangle = \langle v\rangle(t - \Delta\tau^W). \tag{39}$$

In support of this "scattering interpretation," Fig. 3(b) shows excellent agreement of the streaking delay $\Delta\tau_{\rm wake}$ with $\Delta\tau^W_{\rm wake} = \Delta\tau^W_{\rm dyn-ph} - \Delta\tau^W_{\rm sta}$ for photoemission from the Fermi level. We found equally good agreement for emission from individual initial conduction-band states below the Fermi level. For this comparison, we assumed in our streaking calculation that the IR field does not penetrate the solid ($\delta_L = 0$). A detailed discussion of the relation between the Wigner and the streaking delay can be found in Ref. [19].

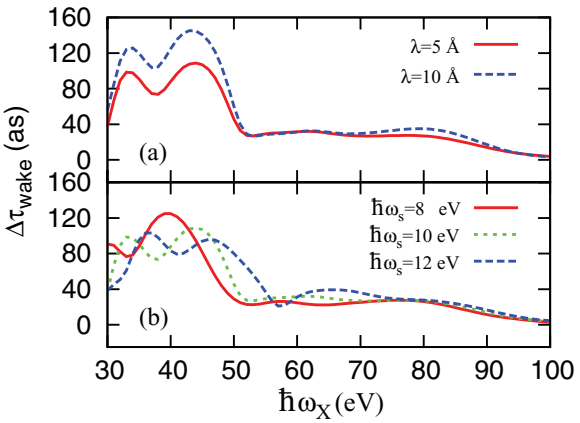

FIG. 4. (Color online) Relative delay $\Delta\tau_{\rm wake}$ as a function of the XUV frequency for $\delta_L = 0$ at different (a) PE mean-free paths λ and (b) surface-plasmon frequencies.

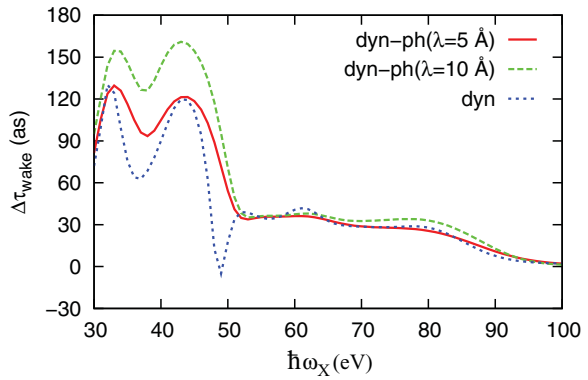

FIG. 5. (Color online) Comparison of the relative delay $\Delta\tau_{\text{wake}}$ as a function of the XUV frequency obtained with $\Sigma_r + \Sigma_{\text{ph}}$ and Σ for the skin depth $\delta_L = 0$.

The effect of the actual IR-skin depth on streaked PE spectra from surfaces is currently debated [2,10,13,24,25]. We therefore found it compelling to study the influence of δ_L on $\Delta\tau_{\text{wake}}$. Our numerical results in Fig. 3(c) show that $\Delta\tau_{\text{wake}}$ is strongly affected by changes in the IR-skin depth if δ_L is smaller than a few mean-free paths λ. Since contributions to the emitted photocurrent are limited to PEs that are released within a few λ from the surface, one would expect $\Delta\tau_{\text{wake}}$ to be less sensitive to δ_L for $\delta_L \gtrsim 2\lambda$ and to stabilize in the limit $\delta_L \to \infty$, in agreement with our numerical results.

Figure 4 shows the dependence of $\Delta\tau_{\text{wake}}$ on the PE mean-free path and the surface-plasmon frequency for $\delta_L = 0$. Increasing λ by a factor of 2 significantly increases $\Delta\tau_{\text{wake}}$ for $\hbar\omega_X \lesssim 50$ eV but has little influence at larger ω_X [Fig. 4(a)]. Our result that, in general, $\Delta\tau_{\text{wake}}(2\lambda) \neq \Delta\tau_{\text{wake}}(\lambda)$ is incompatible with the interpretation [2,25] of the relative delay between photoemission from core and conduction-band levels in tungsten in terms of the PE's average travel time in the solid ($\approx\lambda/\langle v\rangle$). Decreasing ω_s shifts the double-hump structure to the lower ω_X and thus to lower kinetic energies of the PEs, as expected in view of the decreased thresholds for surface and bulk plasmon excitation [Fig. 4(b)].

In Fig. 5 we compare $\Delta\tau_{\text{wake}}$ obtained for $\delta_L = 0$ with either $\Sigma_r + \Sigma_{\text{ph}}$ [cf. Eq. (31)] or Σ [cf. Eq. (32)]. These results show that the imaginary part of the self-energy $\Sigma_i(z, v_z)$ is reasonably well represented by the phenomenological potential $\Sigma_{\text{ph}}(z, v_z)$ for $\lambda = 5$ Å, while noticeable differences between the calculations with the phenomenological and the full imaginary part of the PE self-energy occur near $\hbar\omega_X = 37$ and 49 eV.

V. CONCLUSION

We have calculated the self-energy of a PE that is released from an aluminum surface by an attosecond XUV pulse. By comparing COEs and photoemission delays in IR-streaked PE spectra, including the dynamic electronic self-image potential, with calculations performed in the static limit, we find a significant contribution to the temporal shift $\Delta\tau_{\text{wake}}$ in the photoemission from the metal conduction band. This shift is due to the excitation of bulk and surface plasmons in the metal during and after photoemission and is found to sensitively depend on the XUV frequency as well as on solid-state characteristics, such as the bulk- and surface-plasmon frequencies, the IR skin depth, and the PE transport in the solid. The measurement of streaked electron spectra from dielectric solids may thus be applied to probe solid-state properties—in particular, the solid's ultrafast dielectric response to a moving charge—with unprecedented accuracy. This is supported by our quantitative prediction that wake-induced delays will exceed 50 as. Such time delays can be resolved with contemporary laser technology [1].

The quantitative modeling of time-resolved electron emission from metal surfaces requires a number of approximations that need to be scrutinized, in particular, with regard to the three points mentioned in the second paragraph of Sec. I. We believe that this work provides a viable framework for the future addition of effects that have not been addressed and the removal of some model assumptions we have used. This includes the scrutiny of recoil effects [32] during the propagation of PEs in a solid and nonlocal effects in the electronic self-interaction. We hope that experimental results will soon become available that allow for tests of the simulations presented in this work and serve as a guide to the improved modeling of collective (electronic) excitations in attosecond time-resolved photoemission.

ACKNOWLEDGMENTS

This work was supported by the NSF and the Division of Chemical Sciences, Office of Basic Energy Sciences, Office of Energy Research, US Department of Energy. Numerical computations were performed on the Beocat cluster at Kansas State University.

[1] M. Schultze *et al.*, Science **328**, 1658 (2010).
[2] A. L. Cavalieri *et al.*, Nature **449**, 1029 (2007).
[3] M. Drescher *et al.*, Nature **419**, 803 (2002).
[4] L. Miaja-Avila *et al.*, Phys. Rev. Lett. **101**, 046101 (2008).
[5] A. Kubo *et al.*, Nano Lett. **5**, 1123 (2005).
[6] M. I. Stockman *et al.*, Nature Phot. **1**, 539 (2007).
[7] M. Sukharev and T. Seideman, Nano Lett. **6**, 1123 (2006).
[8] F. Le *et al.*, Phys. Rev. B **76**, 165410 (2007); F. Hao *et al.*, *ibid.* **76**, 165410 (2007).
[9] M. I. Stockman, Phys. Today **64**, 39 (2011).
[10] C.-H. Zhang and U. Thumm, Phys. Rev. Lett. **102**, 123601 (2009).
[11] C.-H. Zhang and U. Thumm, Phys. Rev. A **82**, 043405 (2010).
[12] E. V. Chulkov, A. G. Borisov, J. P. Gauyacq, D. Sánchez-Portal, V. M. Silkin, V. P. Zhukov, and P. M. Echenique, Chem. Rev. **106**, 4160 (2006).
[13] C. Lemell, B. Solleder, K. Tőkési, and J. Burgdörfer, Phys. Rev. A **79**, 062901 (2009).
[14] P. M. Echenique, F. Flores, and R. H. Ritchie, Solid State Phys. **43**, 229 (1990).

[15] J. I. Gersten and N. Tzoar, Phys. Rev. B **8**, 5671 (1973); N. Tzoar and J. I. Gersten, *ibid.* **8**, 5684 (1973).
[16] J. Harris and R. O. Jones, J. Phys. C **6**, 3585 (1973).
[17] J. R. Manson and R. H. Ritchie, Phys. Rev. B **24**, 4867 (1981).
[18] F. J. García de Abajo and P. M. Echenique, Phys. Rev. B **46**, 2663 (1992); **48**, 13399 (1993).
[19] C.-H. Zhang and U. Thumm, Phys. Rev. A **84**, 033401 (2011).
[20] A. A. Lucas, E. Karthueser, and R. C. Badro, Phys. Rev. B **2**, 2488 (1970).
[21] M. Ŝunjić and A. A. Lucas, Phys. Rev. B **3**, 719 (1971).
[22] A. W. Overhauser, Phys. Rev. B **3**, 1888 (1971).
[23] J. Burgdörfer, Nucl. Instrum. Methods **24**/**25**, 139 (1987); C. O. Reinhold and J. Burgdörfer, Phys. Rev. A **55**, 450 (1997).
[24] J. C. Baggesen and L. B. Madsen, Phys. Rev. A **78**, 032903 (2008); **80**, 030901(R) (2009).
[25] A. K. Kazansky and P. M. Echenique, Phys. Rev. Lett. **102** 177401 (2009).
[26] P. M. Echenique, R. H. Ritchie, N. Barberán, and J. Inkson, Phys. Rev. B **23**, 6486 (1981).
[27] S. Hüfner, *Photoelectron Spectroscopy* (Springer, Berlin, 2003), 3rd ed.
[28] R. H. Ritchie and A. L. Marusak, Surf. Sci. **4**, 234 (1966).
[29] J. D. Jackson, *Classical Electrodynamics*, 3rd ed. (Springer, New York, 1999).
[30] H. Ibach, *Physics of Surfaces and Interfaces* (Springer-Verlag, Berlin, 2006).
[31] C. A. A. de Carvalho and H. M. Nussenzweig, Phys. Rep. **364** 83 (2002).
[32] P. M. Echenique, A. Gras-Marti, J. R. Manson, and R. H. Ritchie, Phys. Rev. B **35**, 7357 (1987).